A Simulation Approach for Validation of a Brightband Correction Method

MARCO BORGA

Department of Land and Agro-Forest Environment, University of Padova, Legnaro, Padova, Italy

EMMANOUIL N. ANAGNOSTOU AND WITOLD F. KRAJEWSKI

Iowa Institute of Hydraulic Research, The University of Iowa, Iowa City, Iowa

(Manuscript received 9 September 1996, in final form 27 March 1997)

ABSTRACT

Brightband effects are one of the more important causes of vertical variability of reflectivity and severely affect the accuracy of rainfall estimates from ground-based radar. Monte Carlo simulation experiments are performed to investigate the efficiency of a procedure for the correction of errors related to the vertical variability of reflectivity. The simulation model generates three-dimensional radar reflectivity fields. Brightband effects are simulated through a physically based model of melting-layer reflectivity observations. Sensitivity of the correction procedure for a number of different precipitation scenarios and radar systems is analyzed. Overall, the identification method is found to be a robust procedure for correction of brightband effects. Results indicate a dependence of the effectiveness of the correction procedure on mean altitude and spatial variability of the melting layer.

1. Introduction

An important source of error in rainfall rates derived from radar reflectivity is due to the increase of reflectivity of weather targets in the melting-layer region. This reflectivity enhancement forms the bright band and is primarily due to the rapid increase in the dielectric constant of hydrometeors at the top of the melting layer. Below the brightband peak, melted snowflakes acquire a much higher fall velocity and reflectivity decreases.

Brightband effects are one of the more important causes of vertical variability of reflectivity. Precipitation overestimates up to a factor of 10 may result from bright band (Smith 1986), provided that the radar has the necessary spatial resolution to resolve the brightband layer, which is a few hundred meters thick (Battan 1973). As most weather radars have sufficient spatial resolution only at close ranges, rainfall overestimation due to brightband enhancement occurs mainly near the radar. At medium ranges the bright band compensates for the reduced reflectivity aloft and at longer ranges underestimation dominates. For instance, based on simulations of radar performance during winter months obtained by assuming halfpower beamwidth and beam elevation equal to 1° and 0.5°, respectively, Kitchen and Jackson (1993) show overestimation out to about 80 km and underestimation at farther ranges.

Corresponding author address: Dr. Marco Borga, DTeSAF, AGRIPOLIS, Via Romea, Legnaro, 35020 Padova, Italy.

The influence of the brightband effect on surface radar-rainfall estimates becomes particularly significant when the melting layer is at low altitudes (Collier 1986), or when high elevation angles are used to avoid ground echoes and blocking effects (Bourrel et al. 1994). The importance of removing the brightband effect to improve radar rainfall estimates is well known in hydrology, meteorology, and remote sensing. The major motivation of this study is to improve radar-based precipitation estimates as an input for hydrological models. In this respect, our concern is for long lasting, widespread precipitation events that can cause flooding.

A function, called ''vertical profile of reflectivity'' (VPR), which describes the ratio between reflectivity at a given altitude and reflectivity at the ground, is usually employed to characterize vertical variability. The influence of vertical variability of reflectivity on surface radar rainfall estimates can be corrected if the VPR has been previously identified. The problem of identifying and compensating for VPR effects in real time is not completely solved and is receiving considerable attention, particularly for the brightband case (i.e., Smith 1986; Austin 1987; Klaasseen 1988; Joss and Waldvogel 1990; Koistinen 1991; Gray 1991; Fabry et al. 1992; Kitchen and Jackson 1993; Andrieu and Creutin 1995; Joss and Lee 1995; Hardaker et al. 1995). One way to identify VPR with a radar scanning in PPI mode is to use data from several elevation angles. Harrold and Kitchingham (1975) first proposed a scheme using the ratio of reflectivity measurements taken at two different

elevation angles to correct for VPR. However, the algorithm was numerically unstable and only minor improvement in overall accuracy was obtained. Another method, described by Smith (1986), builds on the work proposed by Harrold and Kitchingham (1975) but attempts to correct only for low-level bright bands. Based on the same principle, Andrieu and Creutin (1995) proposed a method to identify VPR formulated explicitly with regard to the radar equation. The method is based on the assumption of spatial uniformity of VPR. It computes the ratio curve, which is the ratio of reflectivities from scans taken at two different elevation angles and at discrete ranges from the radar. Subsequently, it uses an inverse method to deduce VPR from the observed ratio curve. Identification of VPR allows the computation of a correction factor function, which is dependent upon VPR and radar beam geometry. The correction factor is applied to the reflectivity observations at a given elevation angle to derive reflectivity at the ground. The assumption that VPR is horizontally uniform can be a serious limitation to the application of this technique.

Andrieu et al. (1995) outlined difficulties in direct accuracy analysis of the proposed algorithm and remarked on the need for validation against external information. Such information can be obtained from rain gage measurements or from direct estimates of VPR using a vertically pointing radar. However, both approaches are limited by fundamental differences in the sampling characteristics of the sensors involved (Zawadzki 1975; Kitchen and Blackall 1992; Fabry 1996).

In this study a validation scheme is introduced to test the VPR identification and correction (hereafter referred to as VPR-IC) method proposed by Andrieu and Creutin (1995). This scheme is based on a Monte Carlo framework utilizing synthetic radar reflectivity data including melting layer and related brightband effects. Physically based simulation of the radar measurement process, when combined with simulation of radar sampling and processing of data, allows us to study various sources of uncertainties. The simulation of radar reflectivity measurements includes 1) simulation of the precipitation process itself, including its vertical structure, and 2) simulation of the radar measurement process. A general framework for such simulation is described by Krajewski et al. (1993) and Anagnostou and Krajewski (1996). The VPR-IC method is used to correct for the VPR effect on simulated reflectivity fields affected by bright band. A statistical assessment of the VPR-IC method is conducted by comparing corrected and simulated surface rainfall fields used as a reference. The melting layer and brightband model developed is intended to be a flexible and simple model of an average melting process, able to reproduce realistic space variations of the bright band.

This approach is convenient for performing sensitivity analyses since the reference fields can be assumed as known and factors influencing the shape of the reflectivity profile—such as the mean value of the freezing-level height—can be varied in a controlled manner. Other simulation approaches for the study of weather radar performance along the range have recently been proposed by Fabry et al. (1992) and Kitchen and Jackson (1993). In each study a large set of high-vertical-resolution reflectivity profile measurements was used to simulate scanning radar performance and to analyze errors in surface rainfall estimation due to the radar beam intersecting or overshooting features such as the bright band. Our choice to extend the simulation to the generation of radar observables allows us to account for the influence of different radar parameters and factors such as attenuation and uncertainty in a Z–R relationship. Moreover, the results from a Monte Carlo experiment are statistically valid since long records of data can be generated. Several assumptions have been made to develop the simulation models. Although some of these assumptions may reduce the representativeness of the results, we believe this study provides valuable guidance on what happens in real world operations.

The paper is structured as follows: 1) the procedure for the simulation of radar reflectivity measurements is described, 2) outlines of melting-layer model and assumptions made to simulate scattering properties of melting particles follow, 3) the VPR-IC method is described, 4) the Monte Carlo framework for statistical assessment of the VPR-IC method is presented, and 5) the Monte Carlo experiment results are reported and discussed.

2. Simulation of radar reflectivity measurements

Simulation of radar reflectivity measurement of stratiform precipitation fields involves the following steps.

- simulation of three-dimensional stratiform precipitation patterns,
- simulation of the melting-layer processes, and
- simulation of the radar measurement process.

a. Three-dimensional precipitation model

Three-dimensional precipitation patterns are generated based on a hybrid precipitation model combining 1) a two-dimensional stochastic space–time model (Rodriguez-Iturbe and Eagleson 1987) and 2) a one-dimensional stratiform cloud model. The stochastic space–time model is used to generate the ''true'' surface rainfall patterns. There are several parameters in the rainfall model. Different rainfall climatic regimes can be generated by changing them appropriately. In this work the parameters were tuned to represent stratiform precipitation fields. Rain rates exceeding a threshold value of 11 mm h^{-1} were avoided since rain rates of this intensity could practically never be stratiform (Steiner et al. 1995).

The vertical precipitation structure is entered into the

model based on a cloud model typical for stratiform rainfall. Terrain effects are not included in the model. Accretion and evaporation are neglected as factors affecting vertical variability of precipitation in the rainfall region below the freezing level since the effects of these phenomena are negligible compared to the brightband effect. For this reason, the precipitation rate below the freezing level is assumed to be constant at the surface value. Above the freezing level we assume that there is no liquid water and that the precipitation rate decreases exponentially with height up to the cloud top. The rate of the decrease is derived from work by Fabry et al. (1994a), who observed that the reflectivity of snow decreases at a rate of about 7 dB km^{-1} (with little dependence on precipitation intensity underneath the bright band) at approximately 1.0–1.5 km above the brightband top.

The rainfall model can incorporate variations in time and space for the height of the melting-layer top and hence the brightband top. Data collected in Canada and the United Kingdom (Fabry et al. 1992; Hardaker et al. 1992) shows that the height of the brightband top changes significantly in most stratiform events. For instance, Fabry et al. (1992) claimed that the ''probability that the brightband upper limit is confined within 200 m for a period of 2 h is 50%.'' A dataset kindly provided to us by Frederic Fabry was used to analyze the temporal variability of brightband top height. The dataset consists of a time series of brightband top height, sampled every 2 s and averaged over 30-s time intervals, from 80 storms observed from an X-band vertically pointing radar. Mean, variance, and temporal correlation statistics of the brightband top height were derived from this dataset for each storm. The coefficient of variation ranges from 0.0022 to 0.64 among the different storms. An exponential correlation structure (characterized by a value equal to 0.76 at temporal lag corresponding to 15 min) was chosen to reproduce the temporal lag-correlation values computed over the ensemble of storms after normalization, obtained by taking the ratio with the storm mean value. Following Fabry et al. (1992), space variations were derived from time variations observed at a point by converting time into space through the velocity of the storm system according to the Taylor's hypothesis for turbulence. Based on this approach the spatial correlation function of brightband top height was derived from the observed temporal lag-correlation function. This allowed us to generate two-dimensional stationary Gaussian random fields (Mantoglou and Wilson 1982) to represent the spatial variability of brightband top height.

b. Melting-layer model

As pointed out by numerous investigators (e.g., Gunn and Marshall 1958; Ekpenyong and Srivastava 1970; Yokoyama and Tanaka 1984; Stewart et al. 1984; Fabry et al. 1994a), several mechanisms contribute to the brightband effect. First, it is thought that the aggregation of snowflakes above and perhaps within the melting layer leads to formation of large particles, much larger than typical raindrops (aggregation effect). As these flakes fall below the wet-bulb freezing level they become wet and contain increasing amounts of water. The dielectric constant of melting snowflakes becomes almost that of water and their radar reflectivity is strongly enhanced (melting effect). Furthermore, since water in a melting snowflake is spread throughout the volume of the snowflake, the mixed-phase hydrometeor reflects to the radar like a giant raindrop (density effect). Snowflakes have complicated shapes that deviate significantly from a sphere and may enhance their reflectivity (Atlas et al. 1953) (shape effect). Upon melting, these particles acquire higher terminal velocity, which decreases the concentration of precipitation particles and the radar reflectivity (fall velocity effect). Finally, the sharp decrease of radar reflectivity is also enhanced by the breakup of the melting particles (breakup effect).

Observational and theoretical treatments of the microphysical processes in the melting layer are far from adequate to provide a complete and rigorous explanation for the mechanism causing the bright band. It is, therefore, particularly difficult to quantify the contribution of different processes. Furthermore, it is likely that the relative contribution of these processes is a function of precipitation intensity. Our attention is focused here on modeling bright band in precipitation events heavy enough to cause flooding. It is reasonable to assume that shape effect is more important at weak precipitation rates where small single ice crystals predominate and gradually decrease with increasing precipitation intensity as the average scatterer becomes increasingly spheroid. Furthermore, as stated by Böhm (1991), errors introduced by assuming that particles are spheres are probably negligible for single polarization studies. Aggregation is a more active process at moderate rain rates than at drizzles, due to the greater probability of collision at these rates. Several authors discuss in detail the importance of aggregation and breakup of precipitating particles (e.g., Lhermitte and Atlas 1963; Ohtake 1969; Stewart et al. 1984; Yokoyama and Tanaka 1984; Klaassen 1988; Willis and Heymsfield 1989; Mitra et al. 1990; Fabry et al. 1994a) with conflicting views. Fabry et al. (1994a) suggested that, even at moderate rates, aggregation may account for about 2-dB additional enhancement, on a global value around 14.5 dB. Similar results were obtained by Klaassen (1988).

Fabry et al. (1994a) attempted to provide ''educated guesses'' on the contribution of the different physical processes causing bright band. Based on an analysis of 800 h of vertically pointing X-band radar data, and for a representative brightband profile with reflectivity in the rainfall region around 30 dB*Z*, they suggest that three effects—melting, fall velocity, and density—account for 95% of the ratio of brightband peak reflectivity to rainfall reflectivity.

Based on this background, melting snowflakes are modeled here as spheres. A one-to-one correspondence is assumed between unmelted snowflakes and corresponding raindrops. These are common assumptions in melting layer and brightband modeling (Ekpenyong and Srivastava 1970; Klaassen 1988; Hardaker et al. 1995).

The evolution of the mass fraction of liquid water in the snowflake within the melting layer was taken from Matsuo and Sasyo (1981). These researchers, using a theoretical and observational approach, related the depth in the melting layer h to the melted mass fraction f_m of the particles, which is the ratio of the mass of water produced by melting to the mass of the initial snowflake. Russchenberg (1992) showed that their results can be approximated by the following expression

$$f_m = \frac{1}{2}\left[\sin\left(\frac{h}{H_{\max}}\pi - 0.5\pi\right) + 1\right], \tag{1}$$

where $H_{\max}$ is the distance at which the snowflake is completely melted and can be considered to be the thickness of the melting layer.

The model assumes that the melting-layer thickness increases with precipitation intensity. Larger snowflakes, associated with stronger precipitation, fall faster and take more time to melt. This assumption is based on Klaassen (1988) and Fabry et al. (1994a), who found that the melting layer thickness and the reflectivity below the melting layer ($Z_{e(\text{rain})}$) can be statistically related. The Klaassen (1988) relationship is $H_{\max} = 100Z_{e(\text{rain})}^{0.17}$. The Fabry et al. (1994a) relationship, valid for reflectivity values below the melting layer exceeding 21 dBZ, is $H_{\max} = 140Z_{e(\text{rain})}^{0.17}$. In both, $H_{\max}$ is given in meters and $Z_{e(\text{rain})}$ in dBZ. Since the definitions of brightband top and bottom used by Fabry et al. (1994a) are closer to the height where melting starts and ends, the equation proposed by these authors was chosen to relate the melting-layer thickness with the rain rate below it.

Provided that the mass density of a dry snowflake is known, the mass density of the corresponding melting snowflake is given by

$$\rho_{\text{ms}} = \frac{\rho_s}{1 - (1 - \rho_s)f_m}, \tag{2}$$

where ρ_s is the mass density of a dry snowflake and ρ_{ms} is that of a melting snowflake.

Based on the one-to-one correspondence assumption, a mass conservation equation may be written for each particle as

$$\rho_{\text{ms}}D_{\text{ms}}^3 = \rho_w D^3, \tag{3}$$

where ρ_w is the density of water and D and D_{ms} are the raindrop and the melting snowflake diameter, respectively. Equations (2) and (3) enable calculation of particle size at any stage of melting, provided the dry snowflake mass density is known. Assuming mass flow is constant through the melting layer, the following equation can be written,

$$N_{\text{ms}}v_{\text{ms}}\rho_{\text{ms}}D_{\text{ms}}^3 = N_w v_w \rho_w D^3, \tag{4}$$

which results in

$$N_{\text{ms}} = \frac{v_w}{v_{\text{ms}}}N_w, \tag{5}$$

where N_{ms} is the number of melting snowflakes with diameter D_{ms} and N_w is the number of raindrops with diameter D. Here, v_{ms} and v_w are their fall velocities. Equation (5) shows the concentration of melting snowflakes as larger than the concentration of raindrops because $v_{\text{ms}} < v_w$. It is assumed that all particles fall at terminal velocity and their Reynolds numbers remain constant as they melt. This is because it is assumed that mass remains constant throughout melting and v_{ms} increases as the particle shrinks and becomes denser so that $v_{\text{ms}} \propto 1/D_{\text{ms}}$. Based on this, the following equation can be written as

$$v_{\text{ms}}D_{\text{ms}} = v_w D = v_s D_s, \tag{6}$$

and Eq. (5) can be rewritten as

$$N_{\text{ms}} = \frac{D_{\text{ms}}}{D}N_w. \tag{7}$$

In this way, the size distribution of melting snowflakes may be computed, provided that the drop size distribution of rain and the dry snowflake mass density are known. The determination of the latest variable is accomplished following Hardaker et al. (1995). The mass density (g cm^{-3}) of the snowflake ρ_s is bound by $0.008 \leq \rho_s \leq 0.3$. Here, $\rho_s = 0.008$ is the density of very large snowflakes that contain a large proportion of air, and $\rho_s = 0.3$ is the density for graupel particles. The flake density varies between these two values as

$$\rho_s = \frac{0.02}{D_s^2}. \tag{8}$$

c. Generation of reflectivity measurements

To simulate volume scan reflectivity measurements the following three procedures are involved.

- parameterization of the rain drop size distribution from generated point rainfall rates,
- determination of radar reflectivity and attenuation from parameterized deop size distribution, and
- simulation of the radar sampling process to obtain volume measurements of reflectivity.

To allow a flexible approach for modeling different precipitation types, drop size distribution (*DSD*) is described using a gamma distribution (Ulbrich 1983).

$$N(D) = N_0 D^m e^{-\Lambda D}, \tag{9}$$

where D is the drop size diameter (mm), $N(D)$ the number of raindrops per unit volume per unit size interval (D to $D + \Delta D$), and N_0, m, and Λ are the gamma model's

parameters. Due to the nonunique correspondence between rainfall rate R and the DSD parameters, a statistical parameterization scheme, accounting for the physical variations of DSD, is used. Details are given in Krajewski et al. (1993).

The size distribution of melting particles and dry snowflakes is obtained from Eq. (7). This allows us to generate reflectivity measurements Z_e (mm^6 m^{-3}) and the specific attenuation coefficient k (dB km^{-1}) as follows:

$$Z_e = \frac{\lambda^4}{\pi^5 |K_w|^2} \int_{D_{\min}}^{D_{\max}} \sigma(D_{\text{ms}}) \frac{D_{\text{ms}}}{D} N(D)\, dD, \quad (10)$$

and

$$k = 0.4343 \int_{D_{\min}}^{D_{\max}} Q_t(D_{\text{ms}}) \frac{D_{\text{ms}}}{D} N(D)\, dD, \quad (11)$$

where $\sigma(D_{\text{ms}})$ (mm^2) is the radar cross section of a melting particle of diameter D_{ms} and corresponding to a raindrop of diameter D, $|K_w|^2$ is the dielectric factor of liquid water, λ (cm) is the radar wavelength, and $D_{\min}$ and $D_{\max}$ are the minimum and maximum particle diameters, respectively. Here, Q_t (D_{ms}) is the total attenuation cross section for a melting particle of diameter D_{ms}. Radar and total attenuation cross sections are obtained from the Mie theory (Mie 1908), which allows a realistic representation of scattering in the melting layer, where large hydrometeors are present and the assumption of Rayleigh scattering no longer holds.

The reflectivity of melting particles is computed from the Mie scattering matrix for spherical particles using an average dielectric constant of the ice–air–water mixture. A mixing formula for the dielectric constant computation able to calculate the refractive index of the ice–air–water mixture is the Maxwell–Garnet formula (1904), which treats the mixture as a matrix of homogeneous material that surrounds spherical inclusions of another material. This theory was analyzed by Bohren and Battan (1980) and has been extended by Bohren and Battan (1982) to elliptical inclusions. The Maxwell–Garnet theory deals with a two-component mixture. In the case of melting snowflakes, which consists of three components, the mixing rules must be applied twice, as suggested by Klaassen (1988). In this study, we have computed first the average dielectric constant of the ice–air mixture (snow—where ice was taken as matrix) and then that of the water–snow mixture (where water was taken as matrix).

The reflectivity volume scans are generated by simulating radar beam propagation and integration processes in the three-dimensional precipitation domain. Radar beam geometry and beam pattern effects are accounted for with this simulation model. Details are provided by Anagnostou and Krajewski (1996).

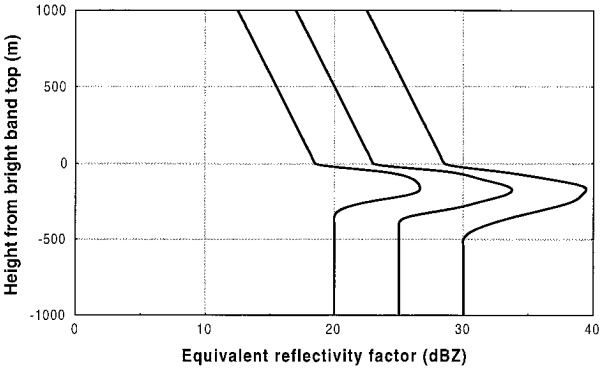

FIG. 1. Mean vertical profiles of reflectivity at X band in and around the bright band based on 250 samples generated by the model for three intensities of rainfall corresponding to 20, 25, and 30 dBZ.

3. Assessment of the simulation model

In this section vertical profiles of reflectivity generated from the model are analyzed. Although the model is built to generate volume scans of radar reflectivity, it can also simulate radar reflectivity measurements made by pointing the beam along the vertical. Simulations generated in this way can be compared with measurements or results obtained from other models, taking into account that the model reproduces spatial and temporal variabilities of bright band in a stochastic way. This makes it difficult to compare results with measurements or simulations representing a particular situation, such as those reported by Lhermitte and Atlas (1963), Klaassen (1988), Willis and Heymsfield (1989), and Hardaker et al. (1995). For this reason, we prefer to use results from a statistical analysis of measured vertical profiles of reflectivity by Fabry et al. (1994a). They reported average profile values for various rainfall intensities below the melting layer.

Vertical profiles were generated using an X-band narrow beam, pointed along the vertical, with a 50-m resolution. In calculations of attenuation and reflectivity, values of maximum and minimum raindrop diameter were set to 0.5 mm and 6 mm, respectively. This drop size range was considered representative of the kind of drops expected in stratiform precipitation. Mean profile values were based on 250 generated samples for reflectivity values below the melting layer at 20, 25, and 30 dBZ. These mean vertical profiles (Fig. 1) can be compared with those reported by Fabry et al. (1994a) in their Fig. 4.7. Overall, the modeled VPRs are quite close to those of Fabry et al. (1994a). The measured peak intensity of the bright band is around 1 dBZ greater in Fabry than in the simulations. Brightband mean thickness is 70 m deeper in the actual data than in the simulations. In Fabry, mean profile values are computed based on profiles characterized by rainfall intensity ranging in a given interval, while in the simulations they are computed for a fixed rainfall rate. Differences in melting-layer thickness depend on this discrepancy

in the averaging process. The slight underestimation of the peak is likely due to assumptions made in modeling the melting layer, namely, aggregation and shape effects on the bright band are negligible. In the region above the melting layer the reflectivity decreases following the observations of Fabry et al. (1994a).

4. Identification of the vertical profile of reflectivity

The algorithm introduced by Andrieu and Creutin (1995) for identification of VPR and correction of its related errors is based on the availability of reflectivity measurements from two antenna elevations. This method requires that the radar equation is formulated taking VPR into account. The basic assumptions of the method are 1) that VPR is homogeneous over the observed area and 2) that the radar reflectivity field may be broken down into two independent functions according to the following scheme:

$$Z(r, y) = Z_0(r)z(y), \tag{12}$$

where r is the horizontal distance from the radar to the target, $Z(r, y)$ is the reflectivity at distance r and altitude y above the radar altitude, $Z_0(r)$ is the reflectivity at ground level, and $z(y)$ is VPR at altitude y. According to these assumptions, the ratio $Q_z(r)$ of two reflectivities at the same radar range r and azimuth and from elevation angles S_1 and S_2 (S_1 being the lowest) is given as follows:

$$Q_z(r, S_1, S_2, z) = \frac{\int_{H_2^-(r)}^{H_2^+(r)} f_{\theta_0}(y)Z(r, y)\, dy}{\int_{H_1^-(r)}^{H_1^+(r)} f_{\theta_0}(y)Z(r, y)\, dy} = \frac{\int_{H_2^-(r)}^{H_2^+(r)} f_{\theta_0}(y)z(y)\, dy}{\int_{H_1^-(r)}^{H_1^+(r)} f_{\theta_0}(y)z(y)\, dy}, \tag{13}$$

where $f_{\theta_0}(y)$ represents the power distribution in the radar beam, which depends on the beamwidth θ_0, $H_i^-(r)$ is the lower limit of the radar beam at elevation i, and $H_i^+(r)$ is the upper limit.

The introduction of this ratio allows us to filter the horizontal variations of the radar reflectivity, the ratio of reflectivity depending only on the radar beam and VPR characteristics. The curve representing the evolution of ratios versus distance is called a ratio curve. To identify VPR, the expression of the ratio is simplified assuming that $z(y)$ is represented by a discrete function, considering n elements ($z_1, \ldots, z_n$) of depth Δy.

The experimental value of the ratio curve at range r is computed by averaging ratios between high and low elevation radar observations for a given azimuth and range interval as

$$Q_z(r) = \frac{1}{n(r)} \sum_{i=1}^{n(r)} Q_{z_i}(r), \tag{14}$$

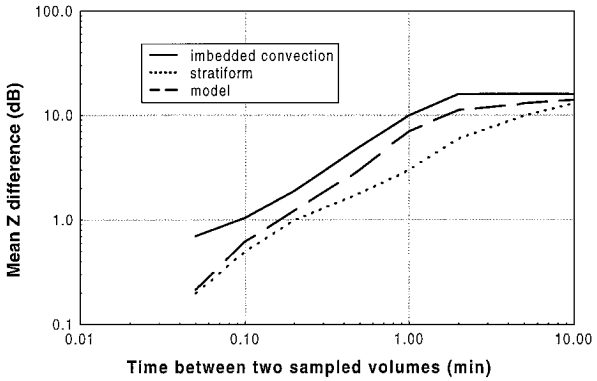

FIG. 2. Gradients of reflectivity vs time as calculated using three months of data from a vertically pointing radar for stratiform rain and rain with imbedded convection and as simulated by using the precipitation model.

where $n(r)$ is the number of resolution cells located within the azimuth and range interval. The objective of the identification method is to determine the VPR that best serves to reconstitute the ratio curve observations with the theoretical model given by Eq. (13). Identifying the VPR is a typical nonlinear inverse problem, which is solved using the algorithm proposed by Tarantola and Valette (1982). Details of this solution are reported by Andrieu and Creutin (1995).

Identification of VPR allows computation of a correction factor function, which depends on the VPR and the beam geometry. Correction for VPR influence is achieved by applying the correction factor function to the reflectivity field taken at a given elevation angle. Doing so, the field is corrected to reproduce, based on the identified VPR, the surface reflectivity field.

5. The Monte Carlo simulation experiment for validation of the VPR-IC procedure

The objective of this study is to establish a validation protocol for the VPR-IC method and to investigate its sensitivity to the spatial variability of the melting layer and to a number of different radar system parameters. To achieve these objectives, a Monte Carlo experiment was designed and performed in which several rainfall scenarios were examined. As an objective constraint for parameter value selection, the rainfall model was calibrated to fit the statistical spatial–temporal structure presented in Fabry et al. (1994b) for stratiform precipitation. This structure represents gradients of reflectivity versus time calculated using three months of data from a vertically pointing radar. Reflectivities were measured at 1-km altitude in rain over a cylindrical volume of 40-m depth and with a diameter of 40 m. The quality of fit resulting from this procedure is illustrated in Fig. 2, where the model results are plotted against the statistical structure computed based on observations by Fabry et al. (1994b).

The rainfall model used in the experiment generates

rainfall fields over a 100 km by 100 km area at 15-min time intervals, with a Cartesian mesh size of 0.5 km by 0.5 km. For each generated rainfield, the model simulates a corresponding three-dimensional radar reflectivity field. The radar is assumed to be located at the upper-left corner of the rainfall domain and operating up to 100-km range. Range resolution is set equal to 1.0 km and half-power beamwidth to 1.0°. We assume that no obstacles reduce the radar's observation capabilities at far ranges. In the experiments, generation of 200 independent realizations, 1 h apart, were found enough to provide robust statistics. VPR identification was performed for every realization, and the correction of radar data was done according to this instantaneous VPR.

Two different precipitation vertical profiles were selected for comparisons: a moderate precipitation profile with the mean value of freezing level set at a height of 1.4 km above radar altitude and a deep precipitation profile with the mean freezing level at 2.4-km height. In each case, the freezing level altitude varied in a range of about 300 m around the mean value. To assess the VPR-IC procedure sensitivity to radar parameters, two different radar systems were considered: one operating at the 5.5-cm wavelength (C-band case) and the other operating at the 10.0-cm wavelength (S-band case).

To examine the sensitivity of the VPR-IC method to the spatial variability of VPR, the simulations involved in scenarios for C band were repeated assuming a freezing level constant in space. In these simulations, only the melting-layer thickness, related to rainfall rate beneath the layer, was considered as variable.

For VPR identification, we used data from the simulated radar volume scans at 1.5° and 3.0°. Corrections are applied to the lower sweep. To smooth out small-scale variations in the precipitation patterns, the reflectivity ratio curves were calculated by averaging data over 15° azimuth sectors. Correction factors were applied to data averaged over the same sectors. The statistical parameters for the VPR-IC method were taken from Andrieu et al. (1995), without fine tuning to the current conditions. The same parameter set is used for both C-band and S-band radars.

The validation protocol is based on comparisons of raw and corrected radar rainfall estimates, taken at the lower elevation (1.5°), and a surface reference value. Radar rainfall is estimated from reflectivity based on the Marshall–Palmer Z–R relationship. We chose not to use simulated surface rainfall generated by the precipitation model as a reference because other sources of errors, such as variations in the Z–R relationship or spreading of the resolution volume with range, could complicate the interpretation of the final results. Therefore, the surface reference values are based on radar rainfall estimates computed from simulated surface reflectivity fields. Two kinds of fields are compared against the corresponding reference fields: 1) fields contaminated by bright band and 2) fields corrected for bright band through the VPR-IC method. Both C-band and S-band cases are considered. An example of rainfall fields obtained from one realization is shown in Fig. 3. Three fields are plotted in this figure: 1) the surface reference field, 2) the lower elevation field (1.5°) before the correction for bright band, and 3) after the correction for bright band. The simulations are carried over a 100 km by 100 km area.

Experimental validation is carried out using two statistics: correlation coefficient ρ and the root-mean-square error relative to the mean reference rainfall rate E_r. These statistics are computed for each realization separately and presented in increasing ρ or decreasing E_r rank order. To avoid any artificial increase in correlation, the statistics are computed for ranges beyond the point where the lower radar beam intercepts the melting layer. Each statistic sample derived from the Monte Carlo experiment is synthesized in a corresponding table, highlighting median and the twenty-fifth and seventy-fifth quartile values.

6. Results

Statistical assessment of results obtained from the Monte Carlo simulation experiment are shown in 1) Figs. 4 and 5 for ρ and E_r, respectively, for the deep precipitation profile, and 2) Figs. 6 and 7, in the same order, for the moderate precipitation profile. A synthesis of these results is provided in Table 1. These results allow detailed analysis of the influence of wavelength and of precipitation profile on 1) the impact of bright band on radar rainfall estimation, and 2) the effectiveness of the correction algorithm.

Wavelength has a noticeable influence on the magnitude of brightband effect. Discrepancies between bright band-contaminated and reference rainfall fields are greater at S band than at C band for both precipitation profiles. Relative root-mean-square error increases around 47%–51% for the S-band case over the C-band case. These differences are due to 1) attenuation on C-band radar signals, 2) the greater sensitivity of a C-band radar than a similar S-band systems, and 3) departure from Rayleigh scattering at the shorter wavelength. When the radar beam travels for some distance along the bright band, severe attenuation, amounting to several times the value found in the rain below, is encountered (see also Joss et al. 1974). This effect is particularly important for C-band radar (Borga et al. 1995). Lack of sensitivity at S band can result in striking differences at altitudes above the bright band, where a significant fraction of the reflectivities could be under the minimum detectable radar signal. Furthermore, the effect of departure from Rayleigh scattering at the shorter wavelength in the melting layer produces a more prominent brightband effect at S band than at C band. Hardaker (1991) calculated that the peak effective reflectivity factor in the bright band at S band can be about twice that at C band. To highlight the overall effect of these various causes, reflectivity ratio curves com-

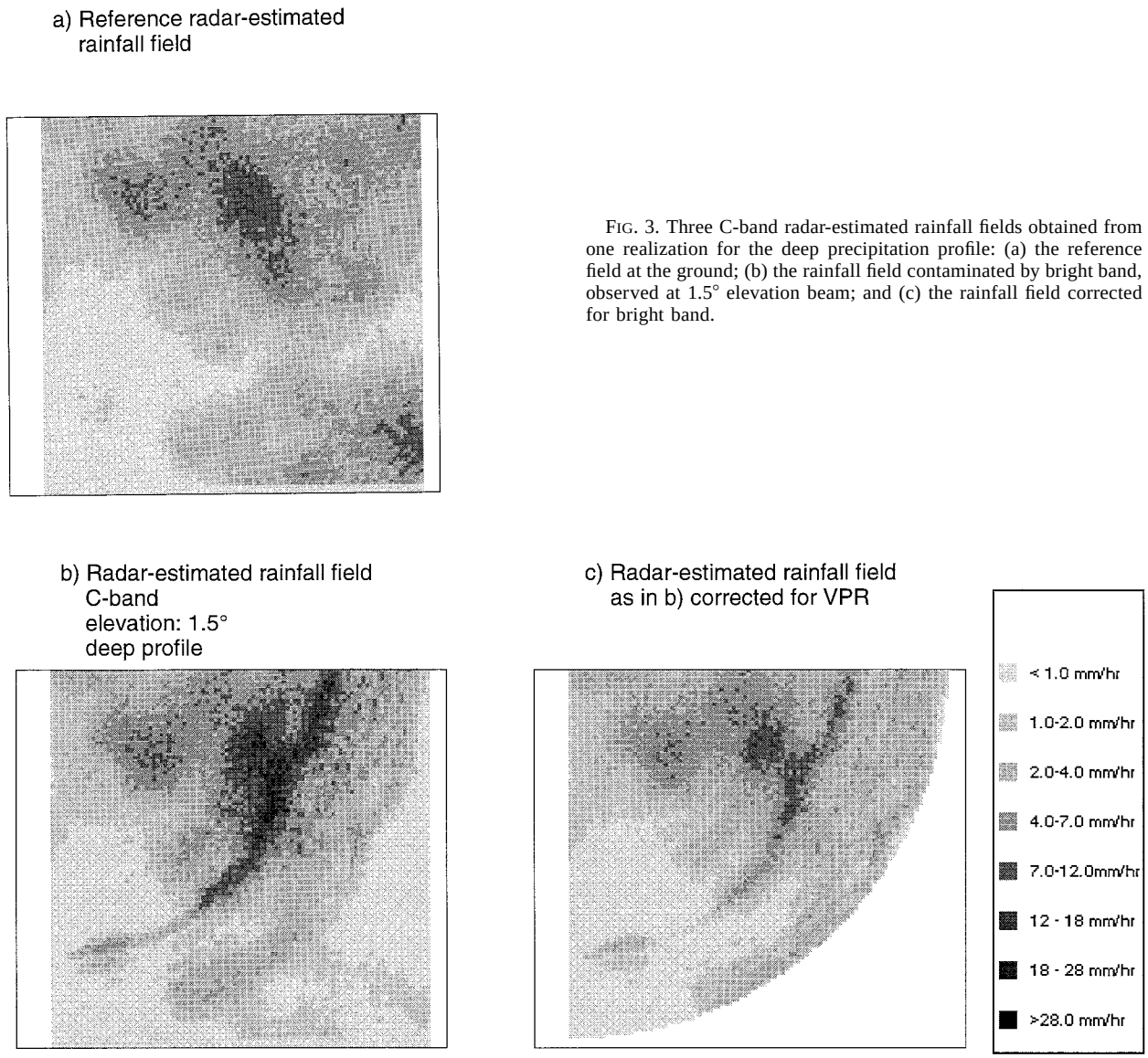

FIG. 3. Three C-band radar-estimated rainfall fields obtained from one realization for the deep precipitation profile: (a) the reference field at the ground; (b) the rainfall field contaminated by bright band, observed at 1.5° elevation beam; and (c) the rainfall field corrected for bright band.

puted from the same realization for C band and S band and for a case of moderate precipitation profile are plotted in Fig. 8. As expected, this figure shows that the ratio curve at S band is more peaked than that obtained at C band.

The VPR-IC procedure improves the agreement between reference and radar data. The relative root-mean-square error is reduced by 40% or more in each case considered. Correlation increases significantly. It is interesting to observe that residual error affecting the corrected fields is remarkably similar for C band and S band. This means that the VPR-IC method correctly applies information provided by the ratio function, indicating a more prominent brightband effect at S band than at C band.

To assess the effect of range, C-band statistical analysis was repeated for two distance intervals from the radar: 1) the range of distances corresponding to radar beam intercepting the bright band and 2) distances at farther ranges from the radar, corresponding to positions of the radar beam sampling the snow region. Syntheses of the resulting statistic sample are reported in Table 2. These results highlight the influence of the mean melting-layer altitude on the magnitude of the error for ranges where the radar beam samples the bright band. As the melting-layer altitude increases, it is intercepted by the radar beam at increasing ranges. The enhancement caused by the bright band becomes less intense because it is spread over a wider annulus. Also, the melting-layer altitude significantly affects the effectiveness of the identification and correction method. The shape of the VPR is better perceived with the melting layer at lower altitudes since in that case the bright band is close to the radar. This improves the accuracy of the identified

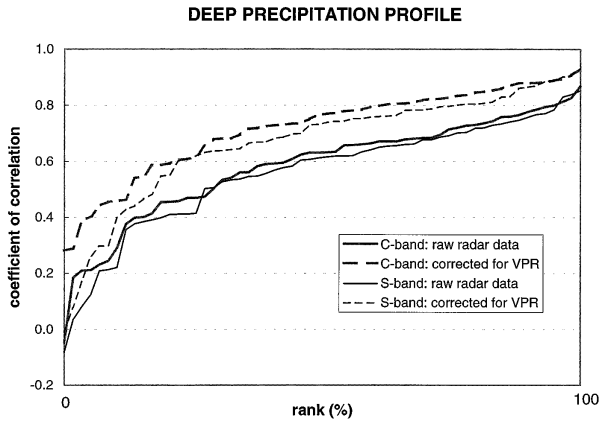

FIG. 4. Correlation coefficients obtained from 200 realizations and ranked according to increasing values, computed between reference fields and radar-estimated rainfall fields taken at 1.5° contaminated by bright band (continuous line) and corrected for bright band (dashed line) for the deep precipitation profile.

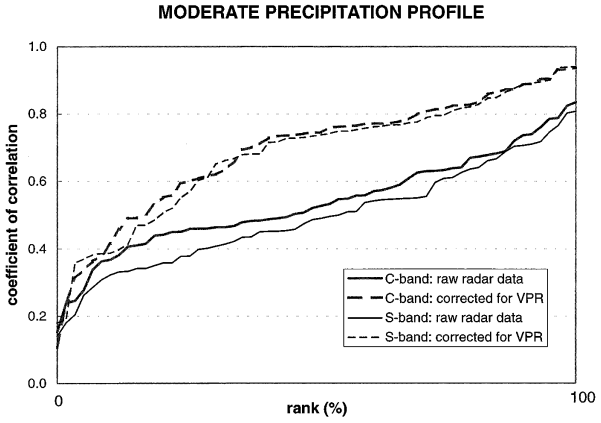

FIG. 6. Same as Fig. 4 except for the moderate precipitation profile.

VPR. Reduction of brightband error is consequently greater in this case than when the melting layer is at higher altitude.

Results reported in Table 2 indicate that correction for the region with radar beam altitude above the melting layer is generally less effective than for the brightband region below. In a number of cases, the application of the VPR-IC method in this region enhances the error. Several factors contribute to this result. According to Andrieu et al. (1995), correct sampling of the higher part of VPR is more difficult than for the lower part since the beam diameter increases with the distance. Therefore, the effectiveness of the identification algorithm deteriorates with increasing distances. These difficulties are compounded by uncertainty affecting basic radar measurements in the snow region, where precipitation echoes are very weak—sometimes under the minimum detectable signal of the radar system. In these situations, ratio values are prone to large fluctuations.

The influence of brightband spatial variability on the effectiveness of the VPR-IC method is illustrated comparing statistical results reported in Table 2 with those reported in Table 3. Table 3 results are obtained for C band with mean freezing level fixed in space at the height of the corresponding precipitation profile. As expected, comparison of results reported in Tables 2 and 3 shows that VPR-IC method effectiveness increases when the spatial variability of brightband decreases. This is not surprising given that the VPR identification procedure is based on the identification of an average VPR function representative of the vertical structure of reflectivity of the investigated domain. Anyway, the sensitivity of the correction method to spatial variations in the brightband top height is not as high as one would expect. This is probably due to smoothing of the small-scale spatial variability obtained by averaging data over

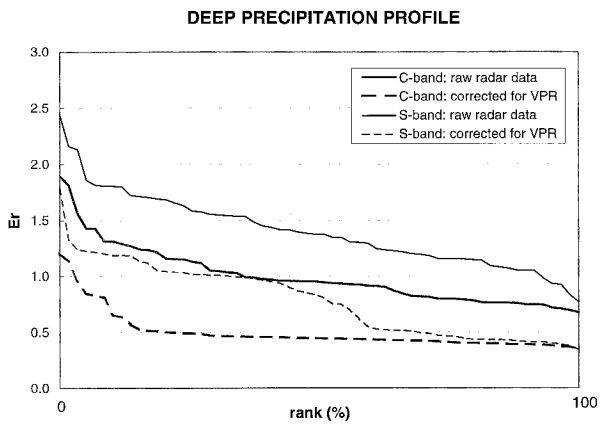

FIG. 5. The E_r statistics obtained from 200 realizations and ranked according to decreasing values, computed between reference fields and radar-estimated rainfall fields taken at 1.5° contaminated by bright band (continuous line) and corrected for bright band (dashed line) for the deep precipitation profile.

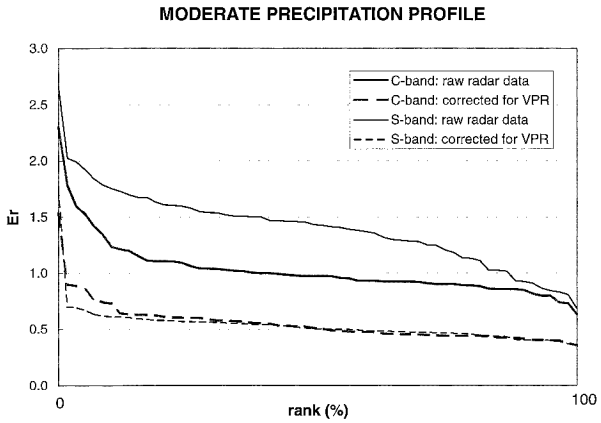

FIG. 7. Same as Fig. 5 except for the moderate precipitation profile.

TABLE 1. Median values and twenty-fifth and seventy-fifth quartiles values (in parentheses) for the distribution of ρ and E_r obtained from the comparison between reference fields and radar-estimated rainfall fields taken at 1.5°, before correction for bright band (case A), and after correction for bright band (case B).

ρ		E_r		
Case A	Case B	Case A	Case B	
C-band radar				
0.52 (0.45–0.63)	0.74 (0.59–0.81)	0.97 (0.90–1.06)	0.51 (0.44–0.60)	Moderate profile
0.63 (0.47–0.71)	0.77 (0.61–0.83)	0.95 (0.79–1.13)	0.44 (0.41–0.49)	Deep profile
S-band radar				
0.48 (0.38–0.61)	0.74 (0.55–0.80)	1.43 (1.18–1.58)	0.50 (0.46–0.57)	Moderate profile
0.61 (0.41–0.69)	0.73 (0.61–0.80)	1.37 (1.15–1.58)	0.82 (0.46–1.02)	Deep profile

1.5° azimuth sectors. Furthermore, note that the sensitivity of the correction is very low in the region with radar beam altitude above the melting layer. In this region, other sources of uncertainty pose some limitations to the effectiveness of the correction algorithm, as noted above. Also, the greater sampling volume in this region tends to smooth the small-scale spatial variability in the VPR.

7. Closing remarks

This work extends an existing model for physically based simulation of radar reflectivity observations to include description of melting layer and related brightband effects. The nature of brightband development makes it particularly difficult to model in detail the melting process and the scattering properties of melting particles. This study attempts to build a flexible and simple model of bright band, one that is able to statistically reproduce the observed spatial variability of melting-layer altitude and thickness. One shortcoming of the model is that it does not consider aggregation and breakup during the melting process. However, VPRs generated by the model do compare favorably with observations from a vertically pointing radar. The merit of this approach is that various factors that influence the shape of the reflectivity profile can be altered in a controlled manner, and error-free radar rainfall simulations can be used to assess the influence of bright band. The use of this simulation approach in a Monte Carlo framework allows assessment of the efficiency of a VPR-IC method.

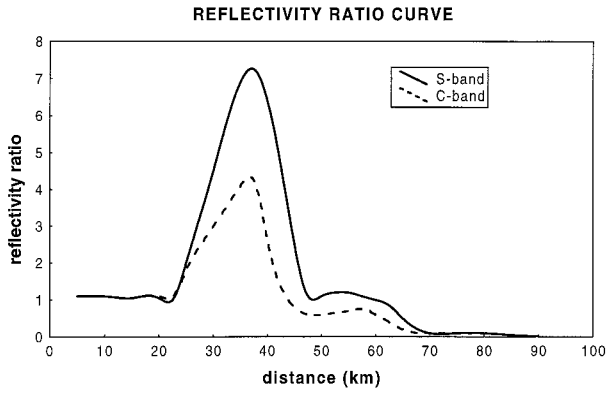

FIG. 8. Experimental reflectivity ratio curves, from the same realization and for the moderate precipitation profile, for S band (continuous line) and C band (dashed line) for an azimuth interval of 15°.

Comparison of results obtained using different radar wavelengths reveals that brightband errors are larger at S band than at C band. However, the residual error affecting the corrected fields is found to be similar for C band and S band.

The Monte Carlo experiment highlighted the influence of mean altitude of melting layer on brightband error and on the effectiveness of the correction method. Better results are obtained for low-altitude bright bands since in this case a better perception of the true shape of VPR is achieved. Correction method effectiveness decreases sharply when the correction is applied to reflectivity measurements from the snow region above the bright band.

Spatial variability in the melting layer significantly affects the quality of the correction obtained by using the VPR-IC method. This is not surprising, given that the identification and correction algorithm is based on the assumption of VPR spatial homogeneity. The sensitivity of the correction method to spatial variability of VPR decreases with range and is remarkably low in the region with radar beam altitude above the melting layer.

It is likely that sensitivity of the VPR-IC method to VPR spatial variability can be reduced by extending its formulation with data from several beam elevations. This should make it possible to identify local VPRs rather than just a single mean VPR. The simulation framework described in this paper can be used for quan-

TABLE 2. Median values and twenty-fifth and seventy-fifth quartiles values (in parentheses) for the distribution of ρ and E_r obtained from the comparison between reference fields and C-band radar-estimated rainfall fields taken at 1.5°, before correction for bright band (case A), and after correction for bright band (case B). Two different interval ranges are considered.

ρ		E_r		
Case A	Case B	Case A	Case B	
Moderate precipitation profile				
0.24 (0.00–0.52)	0.48 (0.23–0.73)	1.21 (1.02–1.32)	0.45 (0.39–0.51)	Radar beam intercepting bright band
0.53 (0.35–0.67)	0.69 (0.45–0.81)	0.77 (0.69–0.82)	0.68 (0.57–0.83)	Radar beam higher than bright band
Deep precipitation profile				
0.29 (0.00–0.56)	0.47 (0.23–0.71)	0.93 (0.85–1.03)	0.55 (0.47–0.65)	Radar beam intercepting bright band
0.56 (0.33–0.69)	0.61 (0.42–0.80)	0.76 (0.67–83)	0.65 (0.55–0.77)	Radar beam higher than bright band

titative assessment of the value of such an extension. The worth of using a vertically pointing radar to detect local brightband height and thickness could also be evaluated in this context.

Acknowledgments. The work of the first author was supported jointly by the Commission of the European Communities, DG XII, Environment and Climate Program, Climatology and Natural Hazards Unit Contract ENV4-CT96-0290, and by the Italian National Research Council Grant 93.02975.PF42. The second and third authors gratefully acknowledge support of the U.S. Army Research Office Grant P-34855-GS-YIP. The authors thank Dr. Herve Andrieu (Laboratoire Central des Points et Chaussees, Division Eau, France) and Dr. Fred Ogden (University of Connecticut) for their comments and discussions, and Dr. Frederic Fabry (McGill University Radar Laboratory, Canada) for providing the brightband height data.

REFERENCES

Anagnostou, E. N., and W. F. Krajewski, 1996: Simulation of radar reflectivity fields: Algorithm formulation and evaluation. *Water Resour. Res.,* **33**(6), 1419–1429.

Andrieu, H., and J. D. Creutin, 1995: Identification of vertical profiles of radar reflectivities for hydrological applications using an inverse method. Part I: Formulation. *J. Appl. Meteor.,* **34,** 225–239.

——, G. Delrieu, and J. D. Creutin, 1995: Identification of vertical profiles of radar reflectivities for hydrological applications using an inverse method. Part II: Sensitivity analysis and case study. *J. Appl. Meteor.,* **34,** 240–259.

Atlas, D., M. Kerker, and W. Hitschfeld, 1953: Scattering and attenuation by nonspherical atmospheric particles. *J. Atmos. Terr. Phys.,* **3,** 108–119.

TABLE 3. Median values and twenty-fifth and seventy-fifth quartiles values (in parentheses) for the distribution of ρ and E_r obtained from the comparison between reference fields and C-band radar-estimated rainfall fields taken at 1.5°, before correction for bright band (case A), and after correction for bright band (case B). Two different interval ranges are considered. Freezing level is fixed in space.

ρ		E_r		
Case A	Case B	Case A	Case B	
Moderate precipitation profile				
0.25 (0.06–0.52)	0.55 (0.28–0.75)	1.15 (1.01–1.25)	0.35 (0.30–0.42)	Radar beam intercepting bright band
0.55 (0.40–0.67)	0.70 (0.46–0.81)	0.79 (0.69–0.82)	0.68 (0.56–0.83)	Radar beam higher than bright band
Deep precipitation profile				
0.31 (0.05–0.60)	0.52 (0.23–0.71)	0.92 (0.84–1.03)	0.47 (0.39–0.54)	Radar beam intercepting bright band
0.60 (0.35–0.70)	0.65 (0.49–0.80)	0.77 (0.67–84)	0.66 (0.53–0.78)	Radar beam higher than bright band

Austin, P. M., 1987: Relation between measured radar reflectivity and surface rainfall. *Mon. Wea. Rev.,* **115,** 1053–1070.

Battan, L. J., 1973: *Radar Observation of the Atmosphere.* University of Chicago Press, 324 pp.

Böhm, J. P., 1991: Sensitivity of computed radar reflectivities on various models of collisional growth. Preprints, *25th Conf. on Radar Meteorology,* Paris, France, Amer. Meteor. Soc., 817–820.

Bohren, C. F., and L. J. Battan, 1980: Radar backscattering by inhomogeneous precipitation particles. *J. Atmos. Sci.,* **37,** 1821–1827.

——, and ——, 1982: Radar backscattering of microwaves by spongy ice spheres. *J. Atmos. Sci.,* **39,** 2623–2629.

Borga, M., E. N. Anagnostou, and W. F. Krajewski, 1995: Validation of a method for vertical profile of reflectivity identification through bright band simulation. *Proc. III Int. Symp. on Hydrological Applications of Weather Radar,* Sao Paolo, Brazil, IAHR, 331–343.

Bourrel, L., H. Sauvageot, J. J. Vidal, D. Dartus, and J. P. Dupouyet, 1994: Radar measurement of precipitation in cold mountainous areas: The Garonne basin. *Hydrol. Sci. J.,* **39,** 369–389.

Collier, C. G., 1986: Accuracy of rainfall estimates by radar, Part I: Calibration by telemetering raingauges. *J. Hydrol.,* **83,** 207–223.

Ekpenyong, B. E., and R. C. Srivastava, 1970: Radar characteristics of the melting layer—A theoretical study. Preprints, *14th Conf. on Radar Meteorology,* Tucson, AZ, Amer. Meteor. Soc., 161–166.

Fabry, F., 1996: On the determination of scale ranges for precipitation fields. *J. Geophys. Res.,* **101** (D8), 12 819–12 826.

——, G. L. Austin, and D. Tees, 1992: The accuracy of rainfall estimations by radar as a function of range. *Quart. J. Roy. Meteor. Soc.,* **118,** 435–453.

——, A. Bellon, and I. Zawadzki, 1994a: Long term observations of the melting layer using vertically pointing radar. Stormy Weather Group Scientific Rep. MW101, McGill University, Montreal, 65 pp.

——, ——, M. R. Duncan, and G. L. Austin, 1994b: High resolution rainfall measurements by radar for very small basins: The sampling problem reexamined. *J. Hydrol,* **161,** 415–428.

Gray, W. R., 1991: Vertical profile corrections based on EOF analysis of operational data. Preprints, *25th. Conf. on Radar Meteorology,* Paris, France, Amer. Meteor. Soc., 824–827.

Gunn, K. L. S., and J. S. Marshall, 1958: The distribution with size of aggregate snow flakes. *J. Meteor.,* **15,** 452–461.

Hardaker, P. J., 1991: The derivation of relationships between bright band parameters and surface rainfall rate at weather radar frequencies. Department of Mathematics Rep., University of Essex, United Kingdom, 9 pp.

——, K. Tilford, C. G. Collier, I. D. Cluckie, and A. R. Holt, 1992: A study of experimentally measured and theoretically derived vertical reflectivity profiles at X-band. URSI Comm. F., Ravenscar, United Kingdom, 2.3.1.–2.3.3.

——, A. R. Holt, and C. G. Collier, 1995: A melting layer model and its use in correcting for the bright band in single polarization radar echoes. *Quart. J. Roy. Meteor. Soc.,* **121,** 495–525.

Harrold, T. W., and P. G. Kitchingam, 1975: Measurement of surface rainfall using radar when the beam intersects the melting layer. Preprints, *16th Conf. on Radar Meteorology,* Boston, MA, Amer. Meteor. Soc., 473–478.

Joss, J., and A. Waldvogel, 1990: Precipitation measurements and hydrology. *Radar in Meteorology.* D. Atlas, Ed., Amer. Meteor. Soc., 577–606.

——, and R. Lee, 1995: The application of radar-gauge comparisons to operational precipitation profile corrections. *J. Appl. Meteor.,* **34,** 2612–2630.

——, R. Cavalli, and R. K. Crane, 1974: Good agreement between theory and experiments for attenuation data. *J. Rech. Atmos.,* **8,** 299–318.

Kitchen, M., and R. M. Blackall, 1992: Representativeness errors in comparisons between radar and gauge measurements of rainfall. *J. Hydrol.,* **134,** 13–33.

——, and P. M. Jackson, 1993: Weather radar performance at long range—Simulated and observed. *J. Appl. Meteor.,* **32,** 975–985.

Klaassen, W., 1988: Radar observations and simulations of the melting layer of precipitation. *J. Atmos. Sci.,* **45,** 3741–3753.

Koistinen, J., 1991: Operational correction of radar rainfall errors due to the vertical profile of reflectivity. Preprints, *25th Conf. on Radar Meteorology,* Paris, France, Amer. Meteor. Soc., 91–96.

Krajewski, W. F., R. Raghavan, and V. Chandrasekar, 1993: Physically based simulation of radar rainfall data using a space–time rainfall model. *J. Appl. Meteor.,* **32,** 268–282.

Lhermitte, R. M., and D. Atlas, 1963: Doppler fall speed and particle growth in stratiform precipitation. Preprints, *Tenth Conf. on Radar Meteorology,* Washington, DC, Amer. Meteor. Soc., 297–302.

Mantoglou, A., and J. L. Wilson, 1982: The turning band method for simulation of random fields using line generation by a spectral method. *Water Resour. Res.,* **18** (5), 1379–1394.

Matsuo, T., and Y. Sasyo, 1981: Melting of snowflakes below freezing level in the atmosphere. *J. Meteor. Soc. Japan,* **59,** 10–24.

Maxwell-Garnet, J. C., 1904: Colors in metal glasses and in metallic films. *Philos. Trans. Roy. Soc. London,* **A203,** 385–420.

Mie, G., 1908: Beiträge zur Optik trüber Medien, speziell kolloidaler Metallösungen (Contribution to the optics of suspended media, specifically colloidal metal suspensions). *Ann. Phys.,* **25,** 377–445.

Mitra, S. K., O. Vohl, M. Ahr, and H. R. Pruppacher, 1990: A wind tunnel and theoretical study of the melting behavior of atmospheric particles. IV: Experiment and theory for snow flakes. *J. Atmos. Sci.,* **47,** 584–591.

Ohtake, T., 1969: Observations of the size distributions of hydrometeors through the melting layer. *J. Atmos. Sci.,* **26,** 545–557.

Rodriguez-Iturbe, I., and P. S. Eagleson, 1987: Mathematical models of rainstorm events in space and time. *Water Resour. Res.,* **23** (1), 181–190.

Russchenberg, H. W. J., 1992: *Ground-Based Remote Sensing of Precipitation using a Multi-Polarized FM-CW Doppler Radar.* Delft University Press, 206 pp.

Smith, C. J., 1986: The reduction of errors caused by bright band in quantitative rainfall measurements made using radar. *J. Atmos. Oceanic Technol.,* **3,** 129–141.

Steiner, M., R. A. Houze Jr., and S. E. Yuter, 1995: Climatological characterization of three-dimensional storm structure from operational radar and rain gauge data. *J. Appl. Meteor.,* **34,** 1978–2007.

Stewart, R. E., J. D. Marwitz, J. C. Pace, and R. E. Carbone, 1984: Characteristics through the melting layer of stratiform clouds. *J. Atmos. Sci.,* **22,** 3227–3237.

Tarantola, A., and B. Valette, 1982: Inverse problems: Quest for information. *J. Geophys.,* **50,** 159–170.

Ulbrich, C. W., 1983: Natural variations in the analytical form of the raindrop size distribution. *J. Climate Appl. Meteor.,* **22,** 1764–1775.

Willis, P. T., and A. J. Heymsfield, 1989: Structure of the melting layer in mesoscale convective system stratiform precipitation. *J. Atmos. Sci.,* **46,** 2008–2025.

Yokoyama, T., and H. Tanaka, 1984: Microphysical processes of melting snow flakes detected by two-wavelength radar. Part I. Principle of measurement based on model calculation. *J. Meteor. Soc. Japan,* **62,** 650–667.

Zawadzki, I., 1975: On radar-rain gage comparison. *J. Appl. Meteor.,* **14,** 1430–1436.